The Astrophysical Journal, 778:162 (11pp), 2013 December 1 doi:10.1088/0004-637X/778/2/162

SOFT X-RAY IRRADIATION OF METHANOL ICE: FORMATION OF PRODUCTS AS A FUNCTION OF PHOTON ENERGY

Y.-J. Chen[1,2], A. Ciaravella[3], G. M. Muñoz Caro[4], C. Cecchi-Pestellini[3], A. Jiménez-Escobar[4], K.-J. Juang[1], and T.-S. Yih[1]
[1] Department of Physics, National Central University, Jhongli City, Taoyuan County 32054, Taiwan
[2] Space Sciences Center and Department of Physics and Astronomy, University of Southern California, Los Angeles, CA 90089-1341, USA
[3] INAF-Osservatorio Astronomico di Palermo, P.za Parlamento 1, I-90134 Palermo, Italy; aciaravella@astropa.unipa.it
[4] Centro de Astrobiología (INTA-CSIC), Carretera de Ajalvir, km 4, Torrejón de Ardoz, E-28850 Madrid, Spain
Received 2013 April 29; accepted 2013 September 29; published 2013 November 13

ABSTRACT

Pure methanol ices have been irradiated with monochromatic soft X-rays of 300 and 550 eV close to the 1*s* resonance edges of C and O, respectively, and with a broadband spectrum (250–1200 eV). The infrared (IR) spectra of the irradiated ices show several new products of astrophysical interest such as CH_2OH, H_2CO, CH_4, HCOOH, $HCOCH_2OH$, CH_3COOH, CH_3OCH_3, $HCOOCH_3$, and $(CH_2OH)_2$, as well as HCO, CO, and CO_2. The effect of X-rays is the result of the combined interactions of photons and electrons with the ice. A significant contribution to the formation and growth of new species in the CH_3OH ice irradiated with X-rays is given by secondary electrons, whose energy distribution depends on the energy of X-ray photons. Within a single experiment, the abundances of the new products increase with the absorbed energy. Monochromatic experiments show that product abundances also increase with the photon energy. However, the abundances per unit energy of newly formed species show a marked decrease in the broadband experiment as compared to irradiations with monochromatic photons, suggesting a possible regulatory role of the energy deposition rate. The number of new molecules produced per absorbed eV in the X-ray experiments has been compared to those obtained with electron and ultraviolet (UV) irradiation experiments.

Key words: ISM: molecules – methods: laboratory: molecular – X-rays: ISM

1. INTRODUCTION

Methanol is a central species in the chemical evolution of interstellar ices. It can be synthesized at very low temperatures by surface hydrogenation reactions on dust grains in cold molecular clouds (e.g., Whittet et al. 2011), and, once formed, it participates in reactions that lead to complex organic molecules via photochemical reactions and other energetic processes (Öberg et al. 2009a). Methanol represents an excellent probe of the chain of events leading to the formation of stars within molecular clouds, and their interaction with cloud remnants (e.g., Leurini et al. 2007). Methanol is typically among the most abundant species and the most abundant organic molecules detected in cometary comae, interstellar ices, and on a variety of bodies at the edge of our solar system (Mumma & Charnley 2011). Methanol abundance varies depending on the environment, ranging from 1% to approximately 30% in interstellar clouds and around protostars (Öberg et al. 2011).

Methanol has been the object of an extensive body of experimental studies both in the gas and solid phases in the astrophysical context. Since the early 1980s, many experiments have been performed to simulate the chemical processing of interstellar ices by energetic processes, exploiting mainly particles and UV radiation. Methanol ice irradiation with UV (Öberg et al. 2009b and references therein), electrons (Bennett et al. 2007), and heavy ions (Baratta et al. 1994; de Barros et al. 2011) are able to produce a great variety of molecules, most of them observed in interstellar icy mantles. Moreover, interest in electron-driven processes involving organic molecules of biological importance has prompted several studies of methanol as the simplest organic molecule that has both methyl and hydroxyl groups. Such studies, in particular those involving low energy electrons (e g., Sullivan 2012), are of importance in astrochemistry since high-energy radiation generates large quantities of these electrons, which then provide the energy for most subsequent reactions.

Despite the importance for prebiotic chemistry, very few studies have been performed using soft X-rays (e.g., Ciaravella et al. 2010; Andrade et al. 2010). Unlike UV photolysis where the energy is released in a single photodestruction event, the interaction of ices with X-rays is a multistep process. The effects of X-ray photons in ices produce ionization/excitation of core electrons of the atoms in the molecules. The ionization or excitation of an inner-shell electron of light elements such as C and O is followed by either normal and resonant Auger decays, with the normal Auger decay active above the ionization threshold. The vacancy in the 1*s* orbital caused by an X-ray photon is filled by an electron from a higher energy level, and the energy released during the event causes the ejection of a second (Auger) electron. Just below the ionization threshold, X-ray photons excite an atom into an excited state accompanied by single electron emission. Such a mechanism is referred to as a resonant Auger effect. The normal Auger mechanism leads to a double ionized molecule that cascades via ionic fragmentation. In the resonant Auger mechanism, the excited molecular state may decay via ionic and, partly, neutral fragmentation (Hempelmann et al. 1999). As a result, X-ray irradiation in different energy bands will promote a variety of ionization/excitation events, fragmentation, and a population of secondary electrons that further interact with the ice contributing significantly to the formation of new species.

Irradiation studies of gaseous CH_3OH near C (287–299 eV) and O (532–546 eV) K-edges have shown the relevance of the normal Auger effect for energies above the ionization threshold in producing doubly or multiply charged species. The experiments by Hempelmann et al. (1999) show that

fragmentation process evidences relevant differences at the C and O K-edges. The irradiation at 292 eV of gas-phase CH_3OH produces fragments caused by C−H bond rupture as testified by the high yields (∼34%) of COH^+ or HCO^+, CH_2OH^+, and H^+ ions, followed, with a lower efficiency, by the C−O bond rupture that produces species such as CH_3^+ (Pilling et al. 2007). Irradiation with 537 eV photons of a CH_3OH ice leads to the break of the C−O and O−H bonds (Andrade et al. 2010). Main photofragments are CH_2^+, H^+, O^+, and H_3^+, along with the negative ions O^- and H^-.

Electron–methanol impact cross sections depend largely on the energy of the impinging electrons. Electron impact ionization of CH_3OH is the dominant inelastic process for energies $\gtrsim$20 eV (e.g., Vinodkumar et al. 2011). Lower energy electrons ($\lesssim$10 eV) lead to dissociative electron attachment, and to molecular excitation. Indeed, the observed formation of products in CH_3OH ices irradiated with electrons of energies below 10 eV demonstrates that electron impact ionization cannot be the sole reaction driving mechanism (Sullivan 2012).

In this work we report experiments performed at the National Synchrotron Radiation Research Center (NSRRC) in Hsinchu, Taiwan. Synchrotron light sources are ideal because of their high intensity and wide wavelength coverage. CH_3OH ices have been irradiated with X-rays, and the new products of the irradiation were studied as functions of the photon energies. The experimental setup is described in Section 2, the products of the irradiation are described in Section 3.1, the effects of the X-ray energy are discussed in Section 3.2, and the comparison with UV and electron irradiations is in Section 3.3. In Section 4 we discuss our results. The relevance of such results for astrochemistry is discussed in Section 5.

2. EXPERIMENTS

The experiments have been performed with the Interstellar Photoprocess System (IPS; Chen et al. 2007). The IPS is an ultrahigh vacuum (UHV) chamber of typical pressure 1–3 × 10^{-10} mbar. The chamber is equipped with a closed cycle He cryostat (CTI-M350) in contact with a sample holder that can reach temperatures as low as 14 K. Two silicon diodes monitor the temperature along the cold finger and at the sample holder position with ±0.1 K accuracy. A gas line system is used for the preparation of gas mixtures. The gas enters the chamber through a capillary where it freezes onto the sample holder. A second needle valve with another capillary is used for deposition of very corrosive gases, e.g., NH_3. A Fourier Transform Infrared ABB FTLA-2000-104 spectrometer equipped with a mercury–cadmium–telluride infrared detector is used to monitor the ice sample. It is connected to the IPS system through a small cylindrical UHV chamber, as to avoid water vapor and carbon dioxide contamination. A Quadrupole Mass Spectrometer (QMS) covering the range of 1–200 amu, with 0.5 amu resolution, provides monitoring of sample purity during the deposition, and measures the photodesorption of the sample during irradiation and the subsequent warm-up phase.

The X-rays used in this study were provided by the Spherical Grating Monochromator beamline at NSRRC, equipped with one grating that covers photon energies from 250 to 1250 eV. The photon flux depends on the photon energy, and it ranges between 5 and 150 $\times 10^{10}$ photons s^{-1}. Figure 1 shows the photon flux distribution in the 250–1250 eV range, measured using an absolute X-ray photodiode (AXUV100G, IRD corporation). The incident photon flux was monitored by an in-line nickel mesh (about 90% optical transmission), calibrated by a traceable photodiode (International Radiation Detectors, Inc.). The spot size of X-ray radiation changed with the energy, and it was measured using fluorescence image of the yttrium aluminum garnet window.

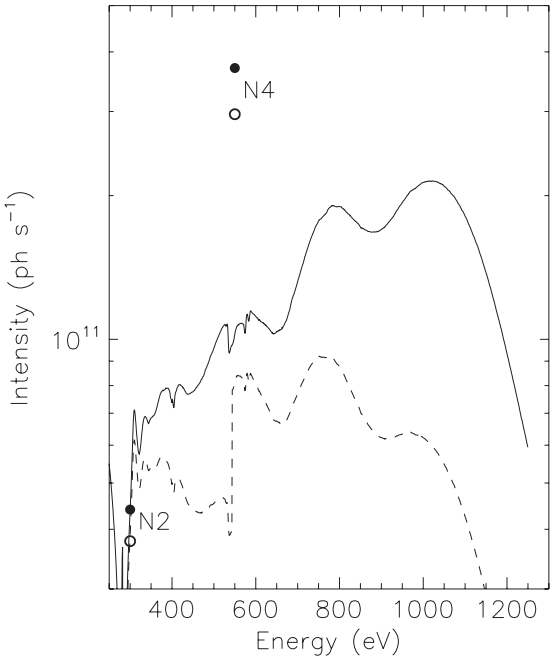

Figure 1. X-ray spectrum of the beamline during the irradiation experiments at 300 eV (black bullet, N2), broad band (solid curve), and 550 eV (black bullet N4). The two circles and the dashed line are the absorbed fluxes in the N4 (550 eV), N2 (300 eV), and broadband experiments, respectively.

Before starting the experiments, the UHV chamber was baked out at 100°C for 48 hr in order to reduce water contamination, then it was cooled down to room temperature, and we waited until the system reached a base pressure of ∼1.3 × 10^{-10} mbar. Before cooling, IR spectra and mass spectra of the KBr substrate were recorded and compared to those at 14 K in order to check for possible contamination of the IPS chamber and sample holder. The gas handling system was also baked out at 120°C before each deposition to eliminate organic and water contamination. Then, when the gas handling system cooled down to room temperature, its base pressure was $\leqslant$1.3 × 10^{-7} mbar. CH_3OH of 99.999% purity was deposited on the KBr substrate at 14 K. After the deposition and before starting irradiation, 20–30 minutes were needed to let the vacuum inside the chamber to reach the base pressure of ∼1.3 × 10^{-10} mbar. During this time, the conditions inside the chamber were monitored by the QMS and the ice by IR spectroscopy. Before and after irradiation, IR spectra were collected with a resolution of 1, 2, and 4 cm^{-1}. To follow the evolution of the gas composition, irradiation was stopped at different times and IR spectra with a resolution of 2 cm^{-1} were collected. After irradiation, the substrate was heated at a rate of 2 K $minute^{-1}$ up to 300 K. During the warm-up, mass spectra were collected continuously while IR spectra were acquired every 10 K with a resolution of 4 cm^{-1}.

Ice samples of pure CH_3OH were irradiated with monochromatic X-ray photons of 300 and 550 eV or with a broadband spectrum in the 250–1250 eV energy range. The spot sizes corresponding to photon energies of 300 eV, 550 eV, and broad band were 10.0, 8.6, and 22.0 mm^2, respectively. The IR spot size, centered on the X-ray spot, was 45 mm^2 for the 300 eV

Table 1
CH_3OH Irradiation Experiments

Exp. N.	Column Dens. (cm^{-2})	Eff. Thickness (μm)	True Thickness (μm)	X-Ray Energy (keV)	Total Irr Time (minute)	Eenrgy Rate (eV s^{-1})
N1	2.08e18	1.08	0.76	0.3–1.2	240	1.1e17
N2	1.96e18	1.02	0.72	0.3	240	1.3e13
N3	1.99e18	1.02	0.73	Blank	240	
N4	2.08e18	1.08	0.78	0.55	70	2.05e14
N5	2.32e18	1.21	0.85	Blank	120	

and broadband experiments and 50 mm^2 for the 550 eV experiment. These differences in the X-ray and IR spot sizes have been taken into account, by multiplying the column densities by the ratio between the IR and the X-ray spots, when computing the molecules produced per absorbed eV in Section 3.3.

The experiments have been performed in two different periods, and the beamline configuration changed. In particular, beamline fluxes during the 300 eV and broadband experiments are lower than those measured during the irradiation at 550 eV. The spectrum of the beamline during the broad band and the fluxes of the 300 and 550 eV experiments are shown in Figure 1. In the figure the black bullets and the solid line are the measured fluxes, while the open circles and the dashed line are the fluxes absorbed by the ices. Column densities have been computed using the CH_3OH band at 1026 cm^{-1}, whose band strength is 1.8×10^{-17} cm $molecule^{-1}$ (Gerakines et al. 1996; D'Hendecourt & Allamandola 1986), and methanol density is 1.020 g cm^{-3} (Bennett et al. 2007).

The ice samples are placed at 45° from the IR and X-ray beams, thus the thickness experienced (effective ice thickness) by X-ray photons and the IR beam is larger by a factor of $\sqrt{2}/2$ as compared to the true (normal) thickness. Table 1 lists the irradiation experiments, the ice column densities, the effective and true ice thicknesses, the X-ray photon energy, the total irradiation time, and the X-ray energy rate at the sample position.

Table 2 provides the absorbed energy values for different irradiation times during the three experiments. The absorbed energies in Table 2 have been computed with the X-ray database tool (http://henke.lbl.gov/optical_constants) based on photoabsorption, scattering, and transmission data by Henke et al. (1993). The absorption of the CH_3OH ice samples is very high near the C and O absorption edges, i.e., about 90% and 80%, respectively. It decreases with the energy to about 50% at 800 eV and become only 20% at 1200 eV.

Table 2
Absorbed Energies

Irrad. Time (s)	N1 (eV)	N2 (eV)	N4 (eV)
16			2.6e15
60	2.4e18	6.8e14	
80			1.3e16
160			2.6e16
180	7.3e18		
300	1.2e19	3.4e15	
340			5.5e16
600	2.4e19	6.8e15	
640			1.0e17
960			1.6e17
1200	4.9e19	1.4e16	1.9e17
1442			2.3e17
1922			3.1e17
2400	9.8e19	2.7e16	
2405			3.9e17
3600	1.5e20	4.1e16	
4205			6.8e17
5400		6.1e16	
7200	2.9e20	8.2e16	
9000		1.0e17	
10800	4.4e20	1.2e17	
12600		1.4e17	
14400	5.9e20	1.6e17	

3. RESULTS OF THE EXPERIMENTS

This section describes the results of the X-ray irradiation experiments in terms of the products of the irradiation (Section 3.1) and the effects of the different X-ray energies (Section 3.2). The efficiencies of the different X-ray energies are computed as the number of new molecules produced per absorbed eV and are compared with those obtained in electron and UV irradiation experiments (Section 3.3).

3.1. Products of the Irradiations

As a result of the irradiation, methanol absorption bands decrease and new bands associated to various photoproducts appear. The molecular assignment of these bands and their strengths are given in Table 3. With the exception of the 1690 cm^{-1} band, the IR spectra of the N1 (broad band) and N4 (550 eV) experiments lead to the same products. Instead, the spectrum of the N2 (300 eV) experiment is the poorest in IR features.

The irradiation experiment N4, using photons of 550 eV, produced the most intense IR bands, and its spectra at different irradiation times are shown in Figure 2. The 1726 cm^{-1} characteristic of CHO-bearing complexes is by far the most intense feature in the experiments. It appears after 16, 60, and 1200 s in N4 (550 eV), N2 (300 eV), and N1 experiments, respectively. Since 16 and 60 s are the shortest irradiation times of the N4 (550 eV) and N2 (300 eV) experiments, we cannot exclude that the band may appear even earlier. The detectability of a product with a band strength of 1×10^{-18} cm^{-1} is less than 1 ML. The 1726 cm^{-1} band together with 1249 cm^{-1} and the blended feature at 1498 cm^{-1}, shown for the N4 (550 eV) experiment in Figure 3, identify the formation of formaldehyde, H_2CO. These bands have also been identified in irradiation experiments with UV photons (Gerakines et al. 1996; Öberg et al. 2009a), 5 keV electrons (Bennett et al. 2007), and energetic ions (Baratta et al. 1994; de Barros et al. 2011). The evolution of the 1726 cm^{-1} band (C=O stretching) during the irradiation as compared to other related bands of H_2CO suggests a contribution from other products. Indeed, after 640 s the appearance of the weak band at 1161 cm^{-1} (C−O stretching of esters, see Figure 2) announces the formation of methyl formate $HCOOCH_3$, most likely a second generation product

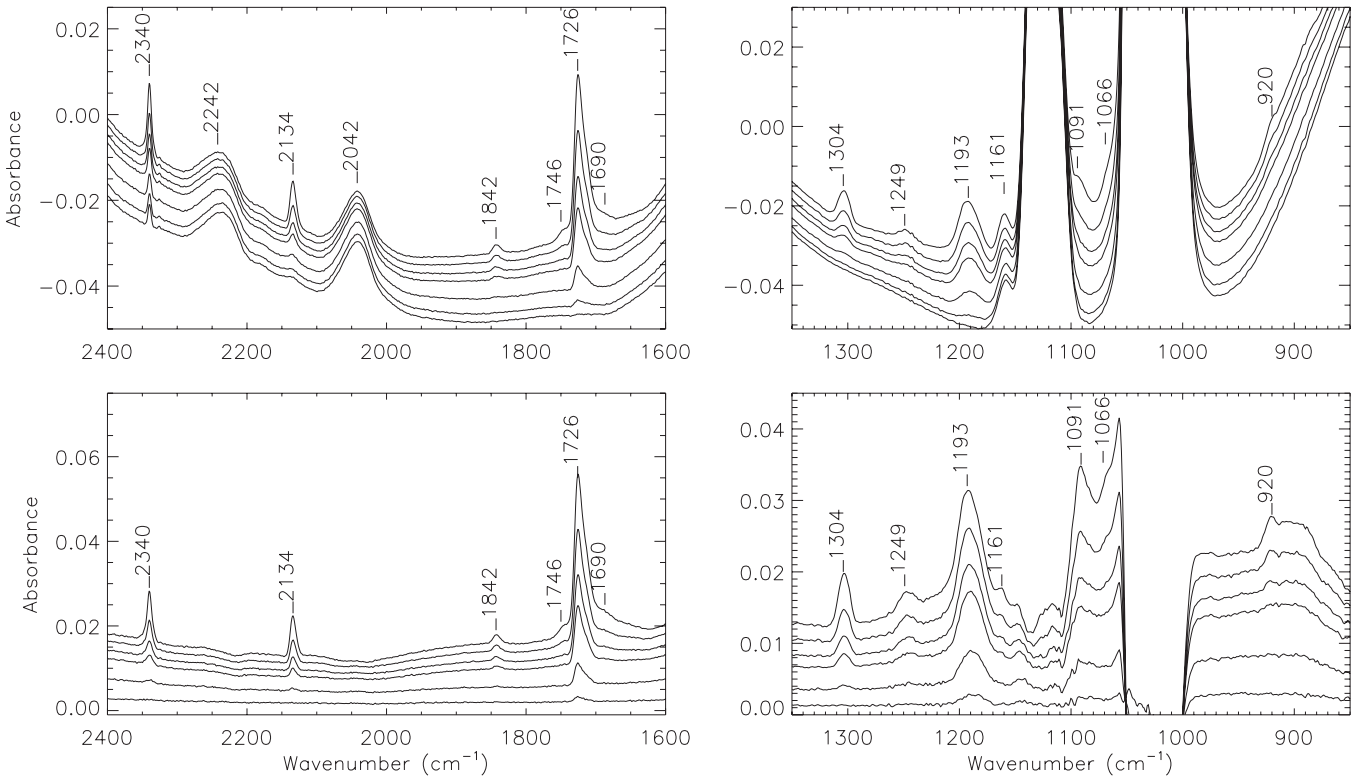

Figure 2. Top panels: IR spectra of CH_3OH ice collected for different irradiation times using 550 eV X-rays (experiment N4). From bottom to top: before irradiation, 80 s, 340 s, 960 s, 1442 s, 2405 s, and 4205 s. Bottom panels: IR spectra shown in the top panel after subtraction of the ice spectrum before irradiation. The spectra have been opportunely shifted.

Table 3
Products of X-Ray Irradiation

IR Band (cm^{-1})	N1	N2	N4	Assignment	Band Strength (cm molecule^{-1})
2340	x	x	x	CO_2	7.6×10^{-17}[a]
2134	x	x	x	CO	1.1×10^{-17}[b]
1842	x		x	HCO	9.6×10^{-18}[c]
1746	x		x	$HCOCH_2OH + HCOOH + CH_3COOH$	
1726	x	x	x	$HCOOCH_3 + H_2CO + HCOOH$	1.2×10^{-17}[d]
1690			x	$HCOCH_2OH$	
1498[B]	x		x	H_2CO	
1304	x	x	x	CH_4	6.1×10^{-18}[e]
1249	x		x	H_2CO	1.0×10^{-18}[f]
1193	x	x	x	CH_2OH	1.6×10^{-17}[g]
1161[W]	x	x	x	$CH_3OCH_3 + HCOOCH_3$	
1091	x		x	$(CH_2OH)_2 + CH_3OCH_3 + CH_3CH_2OH$	
1066[W]	x		x	$HCOCH_2OH$	
1025				CH_3OH	1.8×10^{-17}[e]
920[W]	x		x	CH_3OCH_3	
932–875[W]	x		x	$HCOOCH_3 + (CH_2OH)_2 + CH_3CH_2OH$	

Notes. B: Blended band; W: Weak band.
[a] Yamada & Person 1964.
[b] Jiang et al. 1975.
[c] Milligan & Jacox 1971.
[d] For methyl formate, $HCOOCH_3$ (Wexler 1967; Gerakines et al. 1996).
[e] D'Hendecourt & Allamandola 1986.
[f] Schutte et al. 1993.
[g] Bennett et al. 2007.

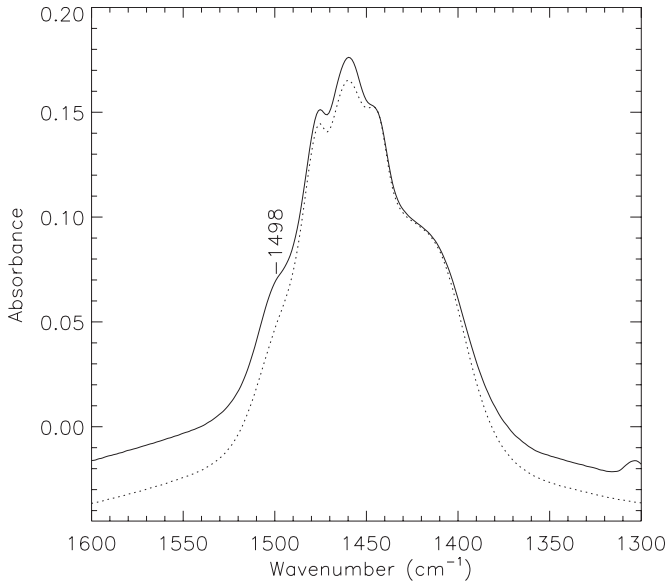

Figure 3. Evolution of the CH_3OH feature in the N4 experiment. Dotted line: before irradiation; solid line: after 4205 s of irradiation. The new blended feature at 1498 cm^{-1} is marked.

formed after H_2CO. A stronger IR band of this product at 1214 cm^{-1} is not observed, but it could be blended with the 1193 cm^{-1} band.

The column densities of the most abundant photoproducts as functions of irradiation time is shown in Figure 4 for the broad band (top panel), 300 eV (middle panel), and 550 eV (bottom panel) experiments. The column densities have been computed from the IR spectra taken at different times during the irradiations and the band strengths listed in Table 3. The contribution to the 1726 cm^{-1} band from species different than formaldehyde is supported by the column densities of photoproducts as functions of irradiation time in the bottom panel of Figure 4. After 640 s of irradiation, the 1726 cm^{-1} band continues to grow upon further irradiation (diamonds) while the formaldehyde abundance, given by the 1249 cm^{-1} band (squares), remains practically constant. The 1726 cm^{-1} band may also have a contribution of CH_3CHO as mentioned by Öberg et al. (2009a), although in our spectra other bands of this product are not observed.

The evolution of the 1726 cm^{-1} band during the warm-up, shown in Figure 5, confirms the contribution from other products: the band decreases with the temperature, but it does not disappear around 70 K as expected for pure H_2CO. The 1249 cm^{-1} band, attributable to H_2CO only, disappears at about 70 K; see Figure 6. The later decrease above 110 K is instead more consistent with the desorption of $HCOOCH_3$. The same behavior is observed in the N1 (broad band) experiment as shown in the left panel of Figure 5. In the N2 (300 eV) experiment, the 1726 cm^{-1} band disappears between 100 and 110 K, suggesting that also in this case the band has a contribution from other species.

The 1726 cm^{-1} band evolves with the irradiation time showing a left shoulder in the N1 (broad band) experiment and both left and right shoulders at 1746 and 1690 cm^{-1} in the N4 experiment (see curves at 14 K in Figure 5). These bands grow with the temperature and disappear around 170 K; see Figure 5. The 1690 cm^{-1} band is not detectable in the N1 (broad band) and N2 (300 eV) experiments even during the warm-up.

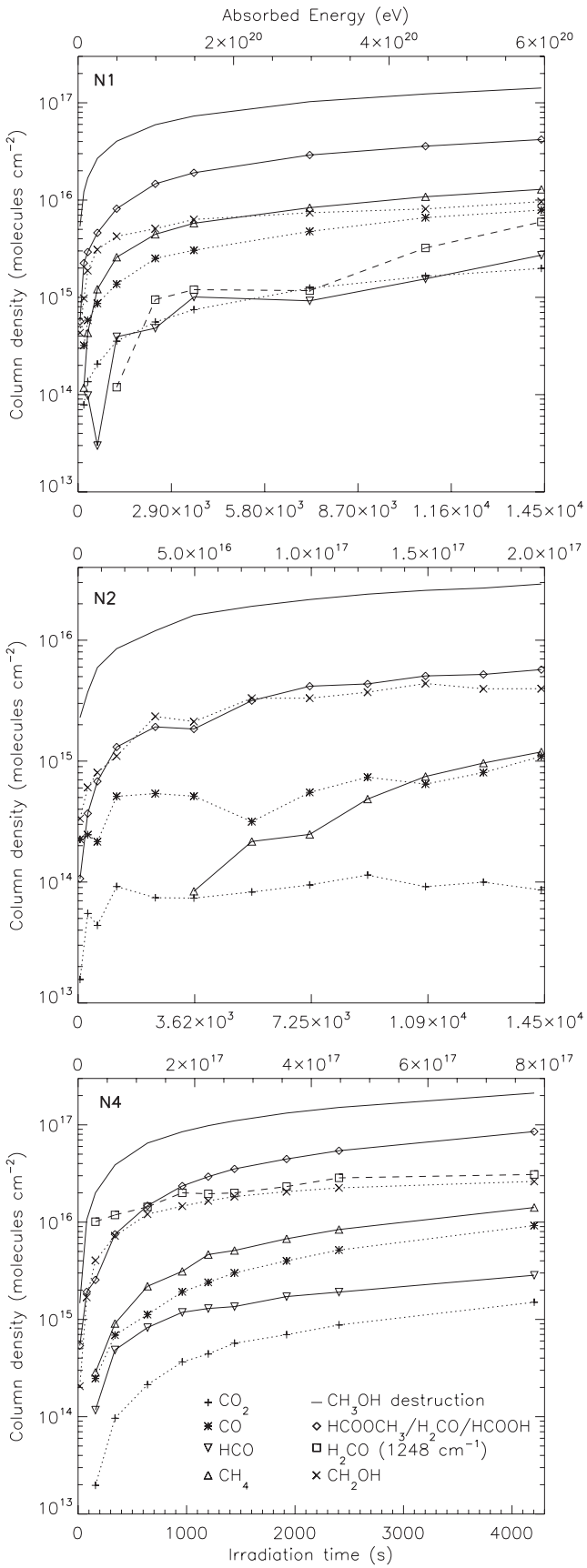

Figure 4. Estimated photoproduct column densities as functions of irradiation time and absorbed energy for the N1 (broad band), N2 (300 eV), and N4 (550 eV) experiments. To account for the difference in the X-ray and IR spot sizes, the column densities of the N1, N2, and N4 experiments should be multiplied by 2.0, 4.5, and 5.8, respectively.

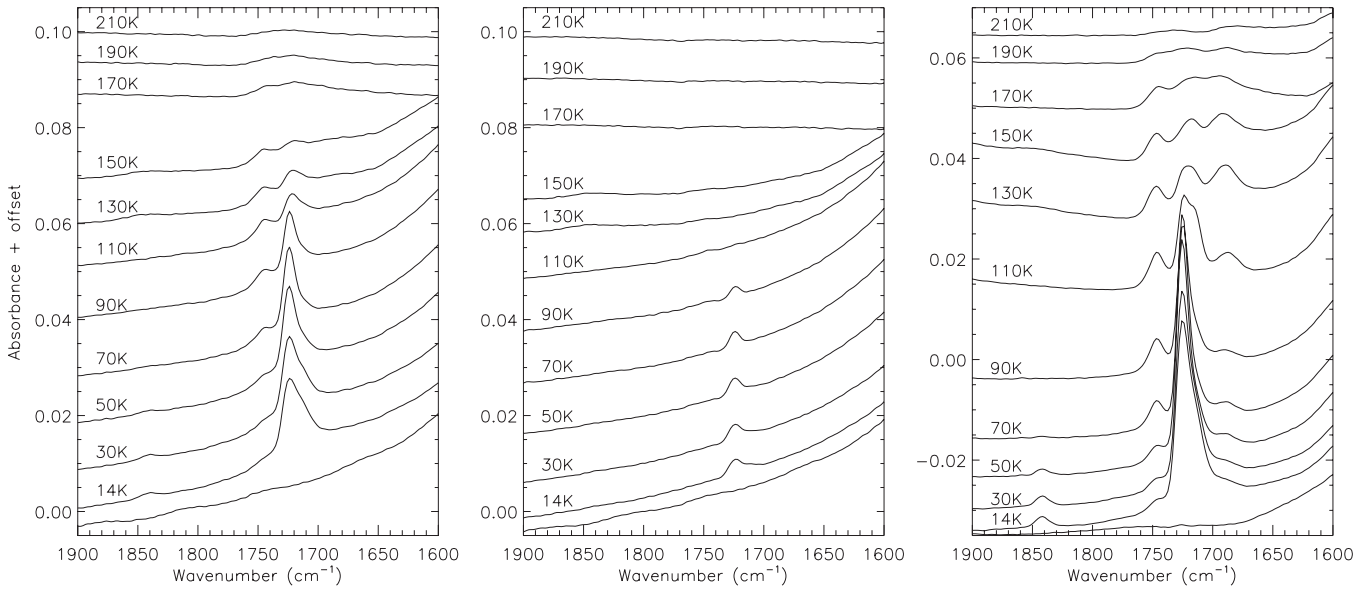

Figure 5. Evolution of the absorbance during the warm-up after the irradiation experiments N1 (broad band, left panel), N2 (300 eV, middle panel), and N4 (550 eV, right panel). The bottom curve in each panel is the absorbance of the sample before irradiation, while the curve at 14 K is the irradiated sample before the warm-up.

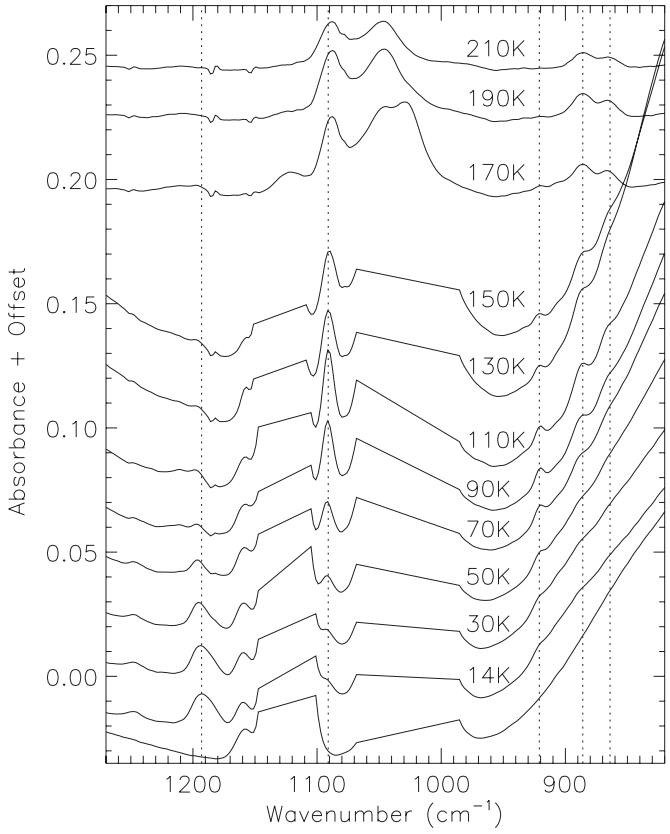

Figure 6. Evolution of the IR spectra in the range of 1270–820 cm^{-1} during the warm-up after the N4 (550 eV) experiment. Methanol bands at 1126 and 1026 cm^{-1} were truncated for a better appreciation of the new bands due to products.

According to the reflection absorption IR spectra by Öberg et al. (2009a), possible carriers of the 1746 cm^{-1} band are glycolaldehyde CH_2OHCHO, formic acid HCOOH, and acetic acid CH_3COOH. The formation of CH_2OHCHO is also supported by the feature at 1690 and 1066 cm^{-1} shown in Figure 2. While the 1746 cm^{-1} band has been reported in UV (Öberg et al. 2009a) and electron (Bennett et al. 2007) irradiation experiments, the 1690 and 1066 cm^{-1} bands have only been detected in electron irradiation of the CH_3OH:CO mixture, where they have been associated to CH_2OHCHO (Bennett & Kaiser 2007).

The 1193 cm^{-1} band associated to CH_2OH appears at the beginning of the irradiation, and it is the second most intense feature common to all the experiments, only surpassed by the 1726 cm^{-1} band. Similar results have been obtained in UV and electron irradiation experiments (Gerakines et al. 1996; Öberg et al. 2009a; Bennett et al. 2007). During the warm-up, in Figure 6, the band starts to decrease at 50 K and disappears around 90 K.

The 1091 cm^{-1} band may have a contribution from ethylene glycol $(CH_2OH)_2$, CH_3OCH_3 and ethanol CH_3CH_2OH as suggested by Öberg et al. (2009a). This band grows with temperature, and it survives up to 210 K; see Figure 6. The broad bump in the range of 932–875 cm^{-1} detected after irradiation in the N2 (300 eV) and N4 (550 eV) experiments clearly includes the feature at 921 cm^{-1} (CH_3OCH_3) and other blended features that have been identified by Öberg et al. (2009a) as produced by $HCOOCH_3$, $(CH_2OH)_2$, and CH_3CH_2OH. As shown in Figure 6, this complex of features also survives up to 210 K.

Dimethyl ether CH_3OCH_3 is a product of our experiments. Its main band at 1161 cm^{-1} overlaps with $HCOOCH_3$, but the features at 921 cm^{-1} that are clearly seen in the difference spectra of Figure 2 confirm its formation. The IR spectra during the warm-up (Figure 6) show an increase of the 921 cm^{-1} feature with the temperature up to 100 K. Then the band decreases but remains visible up to 170 K.

Absorption features of smaller molecules such as the CO_2, CO, and CH_4 are observable in all the experiments at 2340, 2134, and 1304 cm^{-1}, respectively. HCO at 1842 cm^{-1} is only observed in the N1 (broad band) and N4 (550 eV) experiments. The HCO band gradually decreases with temperature and disappears around 70 K. Most of the CO, CO_2, and CH_4 molecules trapped in the methanol ice matrix co-desorb below 150 K.

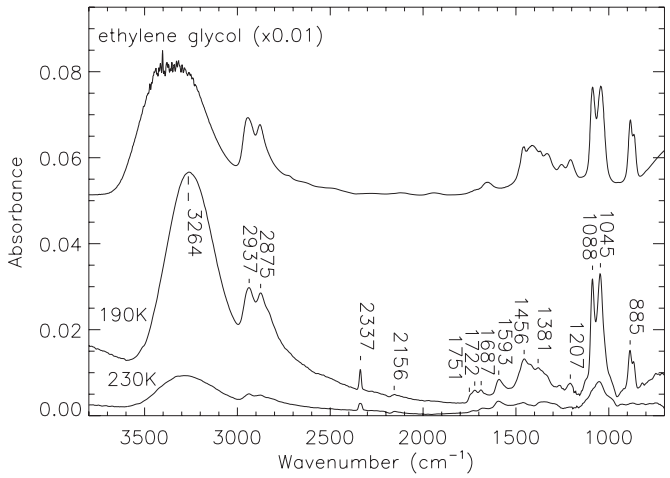

Figure 7. IR spectra of residue at 190 and 230 K obtained in the experiment N4 (550 eV). For comparison, the spectrum of ethylene glycol is also reported. The residue spectra have been opportunely shifted.

Finally, the residue left when CH_3OH has fully desorbed at 190 K is shown in Figure 7. The aliphatic component absorbs in the 3.4 μm region with the main bands at 2937 and 2875 cm^{-1} because of $-CH_2-$ stretching modes, the $-CH_2-$ bend at 1456 cm^{-1}, and the $-CH_3$ symmetric bend at 1381 cm^{-1}. Bands due to functional groups are present at 3264 cm^{-1} related to the H-bonded OH stretch in polymers of alcohols and carboxylic acids, 1722 cm^{-1} for methyl formate with a contribution of 1751 cm^{-1} for α-keto esters, 1687 cm^{-1} for formic acid, and 1593 cm^{-1} that may be an indication of diketones. It was proposed above that ethylene glycol $(CH_2OH)_2$ could be formed during warm-up of the irradiated ice, on the basis of its possible contribution to the band near 1091 cm^{-1}. The growth of this band coincides with the decrease of the CH_2OH band near 1193 cm^{-1}, supporting the ethylene glycol assignment; see Figure 6. For comparison with the residue, the ethylene glycol spectrum is displayed in Figure 7. Several bands in the 190 K residue spectrum have a clear contribution from ethylene glycol, in particular the prominent bands near 1088 and 1045 cm^{-1} and the 885 cm^{-1} band are evidence of this. The absorptions of these bands are drastically reduced in the 230 K spectrum. These infrared bands become very weak after a few days at room temperature, and therefore the residue is not truly refractory.

For comparison, we made a residue using UV irradiation of methanol ice (not shown). The bands around 3200, 2940, and 2880 cm^{-1} are common to the X-ray and UV residues made from methanol ice, and they indicate the presence of OH groups in the aliphatic molecules. However, the fingerprint region is quite different: the UV residue displays less absorption bands and a prominent band at 1718 cm^{-1} that is not present in the X-ray residue spectrum. The presence in the UV residue of the two bands at 1089 and 1047 cm^{-1} indicate that ethylene glycol is also present in the UV residue at 190 K and has sublimated at 230 K.

3.2. Effects of the X-Ray Photon Energy

The results described in the previous section indicate a dependence of photoproduct formation with photon energy. This is evidenced by the non-detection of HCO and α-keto esters in the 300 eV experiment even for the highest absorbed energy of 2×10^{17} eV. On the contrary, HCO is detected in the 550 eV experiment for a similar absorbed energy.

In Figure 8 the column densities of the three most abundant products of Figure 4, 1726 cm^{-1}, CH_2OH, and CH_4, are plotted as functions of the absorbed energy (left column) and photons (right column) in the N1 (broad band), N2 (300 eV), and N4 (550 eV) experiments, respectively. The column densities in Figure 8 have been multiplied by the ratio between the IR and X-ray spot sizes. For the same absorbed energy (1.6×10^{17} eV), column densities of 1726 cm^{-1}, CH_2OH, and CH_4 are 5, 5, and 3 times higher in the 550 eV experiments, respectively. However, for 1726 cm^{-1} and CH_2OH the discrepancy between the two experiments increases with the absorbed energy, with very similar column densities of species produced at early irradiation times. The ratio between the CH_4 column densities produced in the N2 (300 eV) and N4 (550 eV) experiments remains almost unchanged.

One would expect a larger quantity of products in the N1 (broad band) experiment where the absorbed energy is much higher than in the N2 (300 eV) and N4 (550 eV) experiments. In Figure 8 the broadband (N1) irradiation produces about five times less products of 1726 cm^{-1} and CH_2OH than the N4 (550 eV) experiment, although the total absorbed energy (5.9×10^{20} eV) is three orders of magnitude higher. For similar values of absorbed energy ($\sim 10^{18}$ eV), in Figure 8, the column densities of 1726 cm^{-1} and CH_2OH are about two orders of magnitude higher in N4 (550 eV), while CH_4 is not even detectable in the N1 (broad band) spectra.

3.3. Comparing X-Rays with UV and Electron Irradiations

We now compare the number of molecules produced per deposited eV in our experiments with those obtained with 5 keV electrons (Bennett et al. 2007) and UV (Öberg et al. 2009a) irradiation sources. The number of molecules produced per deposited eV in the ice, Ψ, is computed as the ratio of the measured column density N and the total absorbed energy per cm^2, $E_{\rm abs}$:

$$\Psi(t) = \frac{N}{E_{\rm abs}} \text{ molecule eV}^{-1}. \quad (1)$$

It is worth mentioning that the Ψ values vary with the exposure time since the production rate of new species decreases with the absorbed energy. Table 4 lists the Ψ values for some of the irradiation products for X-ray energies at the end of the experiments (this work), 5 keV electrons (Bennett et al. 2007), and UV photons (Öberg et al. 2009a). The column densities of the X-ray experiments have been multiplied by the factors 2.0, 4.5, and 5.8, corresponding to the ratio of the IR to X-ray spot sizes in the N1 (broad band), N2 (300 eV), and N4 (550 eV) experiments, respectively. The irradiation at 550 eV gives the highest number of molecules per absorbed eV as compared to 300 eV and broadband experiments.

In the experiment by Bennett et al. (2007), an area of 3 cm^2 of a methanol ice is irradiated for 1 hr with 5 keV electrons. Each electron transfers to the ice $\sim$390 eV corresponding to an energy flux of approximately 2×10^{14} eV s^{-1} similar to our N2 (300 eV) and N4 (550 eV) experiments. The total energy transferred to the ice is 2.3×10^{17} eV cm^{-2}. The column densities of the products are from Table 4 of Bennett et al. (2007), scaled appropriately in order to use the same band strengths (see Table 3) as for the X-ray experiments. The production of CH_2OH reach a maximum value (0.6×10^{16} cm^{-2}) at about 1300 s and then starts decreasing; see Figure 8 of Bennett et al. (2007). For this species, we also report the Ψ values after 1300 s of irradiation.

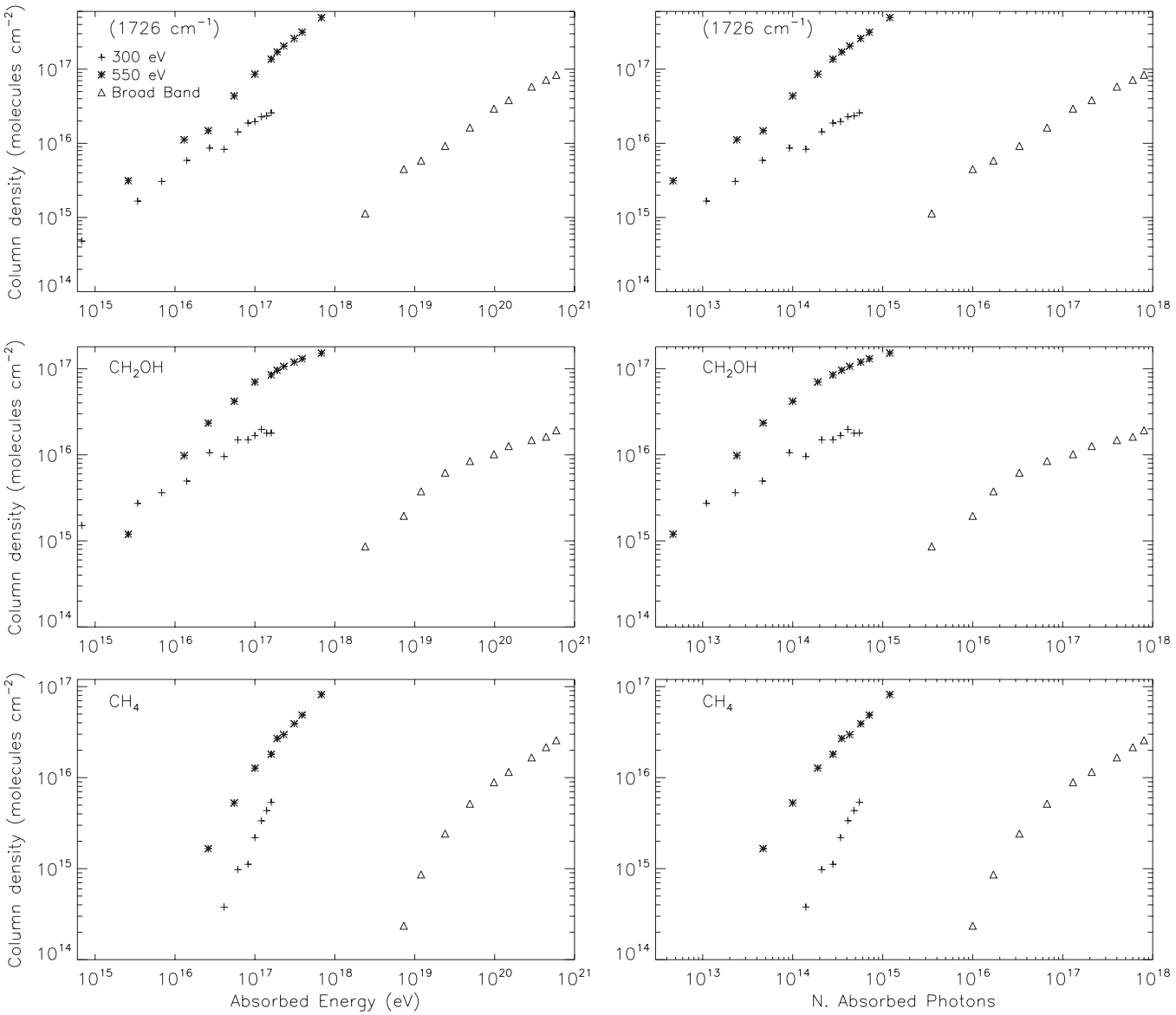

Figure 8. Column densities for 1726 cm^{-1} ($HCOOCH_3$ + H_2CO + HCOOH), CH_2OH, and CH_4 as functions of the absorbed energy (left column) and photons (right column) in the N1 (broad band, triangles), N4 (550 eV, asterisks), and N2 (300 eV, crosses) experiments. In order to take into account the difference between the X-ray and IR spot sizes (see text), the column densities of the N1, N2, and N4 experiments have been multiplied by 2.0, 4.5, and 5.8, respectively.

Table 4
Number of Molecules Produced per Absorbed eV in X-Ray, 5 keV e$^-$, and UV Experiments

IR Band (cm^{-1})	Species	Number of Molecules per Deposited eV				
		N1	N2	N4	(5 keV e$^-$)[a]	UV[b]
2134	CO	2.3(−6)	0.003	0.005	0.003	0.004
1842	HCO	7.9(−7)	0	0.002	0.001	0.0005
1726	$HCOOCH_3$[c]	1.2(−5)	0.014	0.049	0.006	...
1304	CH_4	3.7(−6)	0.003	0.008	0.014	0.01
1249	H_2CO	1.7(−6)	0	0.018	...	0.007–0.01[d]
1193	CH_2OH	2.8(−6)	0.009	0.015	0.07–0.022[e]	0.001–0.006[d]
1025	CH_3OH	−4.2(−5)	−0.069	−0.123	−0.077	...

Notes.
[a] Bennett et al. 2007.
[b] Öberg et al. 2009b.
[c] Used a band strength of 1.8×10^{-18} cm molecule^{-1}.
[d] The two values are computed for two values of the UV fluence, see Section 3.3.
[e] The two values are computed for two values of the absorbed energy, see Section 3.3.

Öberg et al. (2009a) irradiate a CH_3OH ice that is 21 ML thick at 20 K with a H I Lyα lamp for 6 hr. The total energy furnished to the ice is 2.376×10^{17} photons cm^{-2}. Assuming an average photon energy of 10 eV and an absorption of 12%, corresponding to an average cross section of 6×10^{-18} cm^{-2} in the 120–160 nm range of the UV lamp (Cruz Diaz et al. 2013), the total absorbed UV energy is $E_{abs} \sim 2.85 \times 10^{17}$ eV cm^{-2}. The column densities of the UV products are computed using the column densities in a percentage of the initial CH_3OH from Figure 16 of Öberg et al. (2009a). The initial CH_3OH column density has been computed assuming that 1 ML $\sim 10^{15}$ molecule cm^{-2} (Öberg et al. 2009b). The obtained values have been scaled in order to obtain the same band strengths as in Table 3 of this work. The two values for H_2CO and CH_2OH are obtained using the column densities at the end of the irradiation and just before the saturation level is reached. In particular, the column densities before saturation are $\%N_{CH_3OH} = 7.5$ and 1.5 for H_2CO and CH_2OH, respectively. These values correspond to UV fluence of 1×10^{17} for H_2CO and 0.4×10^{17} cm^{-2} for CH_2OH; see Figure 16 of Öberg et al. (2009a).

The number of molecules produced per absorbed eV in our experiments are similar to those obtained in the reported electron experiment, with some density columns being larger and some being smaller. In the case of $HCOOCH_3$, the column density per eV synthesized by X-ray photolysis is more than one order of magnitude larger than in the electron experiments. Data in Table 4 also suggest a lower product efficiency by UV irradiation.

4. DISCUSSION

The results of the X-ray experiments show that the abundance of the new products depend on the impinging photon energy, the total absorbed energy, and the energy deposition rate: (1) during each experiment the concentrations of newly formed species increase with the absorbed energy; (2) the monochromatic irradiation at 550 eV provides more products than the irradiation at 300 eV, testifying to the role of photon energies; and (3) the broadband irradiation experiment shows a marked decrease per unit energy in the product abundances despite the wider range of the photon energies, suggesting a regulatory role of the energy deposition rate. The energy deposition rate of the broadband irradiation is more than two orders of magnitude larger than in the monochromatic experiments at 300 and 550 eV.

These results depend on the nature of X-rays interaction with the ice. X-rays deposit their energy through the combined interactions of photons and electrons with the ice material. The ionization of an inner-shell electron as a consequence of the absorption of an X-ray photon is followed by the production of photoelectrons, which in turn interact with the ice. A significant contribution to the formation and growth of new species is given by secondary electrons, whose energy distribution depends on the X-ray spectrum.

The differences between the two monochromatic experiments may be related to the different induced photofragmentation channels of CH_3OH: 300 eV photons promote the rupture of the C-H bond favoring the formation of species such as CH_2OH rather than CH_4, while 550 eV photons tend to break C-O bonds (Hempelmann et al. 1999). Such different photofragmentation of CH_3OH induced by 550 and 300 eV photons may explain the different efficiency in inducing the formation of new species at low energies, with products such as CH_2OH favored in the N2 (300 eV) experiment, and CH_n^+ species in the N4 (550 eV) experiment. At higher energies, the effects provided by secondary electrons tend to dominate the product formation. The photon energies close to C (288 eV) and O (537 eV) 1*s* resonance edges, as in the N2 (300 eV) and N4 (550 eV) experiments, produce a bimodal distribution of ejected electrons, a low energy primary photoelectrons population of about 10 eV, and a very energetic Auger component. Typical energies of Auger electrons from O and C atoms are about 530 eV and 280 eV, respectively. Thus, the more energetic secondary electrons arising from 550 eV photoionizations produce a larger number of ionization/excitation events, making such photons more efficient than 300 eV photons. Low energy electrons can also be important in driving the chemistry: three resonance peaks at energy below 12 eV favor the methanol anion dissociations (Bouchiha et al. 2007, and references therein) onto ions and radicals that in turn promote formation of new species. At higher energies, the electron impact methanol ionization becomes more efficient (Harris et al. 1995; Rejoub et al. 2003; Vinodkumar et al. 2011). Cross sections for electron-impact ionization of CH_3OH in the range from 13 eV to 1 keV has a broad peak around 80 eV (Rejoub et al. 2003). Thus, electrons of 20 eV are as efficient as those of 900 eV in ionizing methanol.

Photoproducts also increase with the absorbed energy during the broadband irradiation. Nevertheless, the much higher absorbed energy in the broadband irradiation does not correspond to a greater amount of photoproducts. After the first 60 s of irradiation with broad band, the ice absorbs about three times the energy absorbed in 4205 s at 550 eV. The column densities of the new products are three orders of magnitude less than in 550 eV experiment. These results clearly suggest that the absorbed energy is not the only driver of the chemistry. The main differences with the monochromatic experiments are the spectral distribution and the intensity of the impinging radiation. The rate at which the energy is absorbed in the broadband (N1) experiment, 4.1×10^{16} eV s^{-1}, is about 250 times higher than in the 550 eV (N4) experiment. Correspondingly, the total number of absorbed X-rays photons during the N1 experiment, 8.0×10^{17}, is about three orders of magnitude higher than in the N2 (5.5×10^{14}) and N4 (1.2×10^{15}) irradiations. The number of primary electrons ejected in the ice matrix is roughly twice that of photons. Of the total absorbed energy (5.9×10^{20}eV), about 87% (80%) comes from photons above 550 eV (600 eV). The population of primary photoelectrons is therefore dominated by electrons of high energy, higher than those produced in the N2 (300 eV) and N4 (550 eV) experiments. These electrons should be efficient in ionizing/exciting the methanol molecules and at the end producing a population of low energy electrons. Thus, the result should be an increased production of new species.

On the other side, the very large energy deposition rate in the broadband experiment has the effect of producing a large amount of secondary electrons, whose concentration is at least two orders of magnitude larger than in the monochromatic experiments. First, such a large electron concentration may have destructive effects on the newly formed species. Second, the electron-electron elastic scattering may dominate over inelastic collisions, leading to the heating of the ice. Destructive effects are supported by the results of irradiation experiments with 0.1–2 keV electrons of ices containing organic compounds (Barnett et al. 2012).

Finally, a high-energy flux may induce large ice desorption, significantly reducing the amount of new products. The QMS spectra taken during the broadband (N1) irradiation show

smaller desorption than in the N4 (550 eV) experiment. Higher energy photons penetrate deeply in the ice, and as a consequence the portion of the primary photoelectrons energy converted in heating of the ice does not causes desorption. The inelastic mean free path of the electrons in the methanol ice can be estimated from the inelastic cross section of about 1.1×10^{-16} cm^2 (Vinodkumar et al. 2008) for electrons of 1 keV, resulting in about 0.4% of the ice thickness (about 1 μm, see Table 1).

Further experiments are needed to understand the mechanisms that limit the abundance of new species in X-ray irradiated ices.

5. CONCLUSIONS AND ASTROPHYSICAL IMPLICATIONS

Three irradiation experiments on methanol ice were performed using two monochromatic energies at 300 and 550 eV, close to the 1*s* resonance edges of C and O, respectively, and a broad energy spectrum ranging from 250 to 1200 eV. The IR spectra of the irradiated ices along with those taken during the warm-up process show IR features of several molecules of astrophysical interest such as CH_2OH, H_2CO, CH_4, HCOOH, $HCOCH_2OH$, CH_3COOH, CH_3OCH_3, $HCOOCH_3$, and $(CH_2OH)_2$, as well as HCO, CO, and CO_2. The formation of the new species occur through a peculiar chemistry in which both photons and electrons concur in the deposition of the energy provided by the X-ray primary spectrum. Nevertheless, such species are similar to those obtained in UV and particle irradiation experiments.

Within a single experiment, the abundance of the products increases with the absorbed energy. Monochromatic experiments also show that product abundances also increase with the photon energy. Such a trend is not found when the irradiation is performed exploiting a broad X-ray spectrum, occurring at a deposition rate few orders of magnitude larger than in the monochromatic experiments. The intensity of the photon spectrum may be responsible for the observed decreased efficiency, although further investigations are still needed.

The efficiency of X-rays in inducing a formation of new products has been evaluated by computing the number of new molecules produced per absorbed eV. X-rays of 550 eV are the most efficient among the exploited photon energies. The comparison with 5 keV electrons (Bennett et al. 2007) and UV photon irradiation (Öberg et al. 2009a) shows that for some species X-rays are more efficient and for others they are not. This aspect needs further investigations.

X-rays are an important component of the radiation field in several astrophysical environments. Such energetic radiation plays a central role in the very first stages in the life of solar-type stars. High-energy radiation, even if it is a relatively small fraction of the total energy available, can indeed influence significantly the stellar system formation and the subsequent evolution. Young solar type stars emit X-rays at a level that is 3–4 orders of magnitude higher than the present-day Sun, during both the pre-main-sequence phase when the emission is dominated by intense flares (e.g., Feigelson et al. 2003) and the first phases of the main sequence when a solar-like star has an X-ray luminosity in the range of 10^{29}–10^{30} erg s^{-1}. Around 100 Myr, the X-ray luminosity of a solar-type star starts to decrease, and at about 5 Gyr it reaches the (average) value of $\sim 10^{27}$ erg s^{-1}, today's quite Sun. Thus, X-ray emission is an important spectral component of a young solar-type star: for a 100 Myr old star the X-ray flux is larger than the extreme UV one, and their ratio remains within a factor of two for stars as old as 1 Gyr; for today's Sun the ratio is about 0.25 (e.g., Ribas et al. 2005). Although such a copious X-ray emission must have processed circumstellar materials, only recently has some attention been paid to the effects induced by irradiating interstellar/circumstellar matter analogues in this spectral range. Such studies are relevant for a large number of astronomical processes, since molecular ices are present in a variety of astronomical regions: in the Solar System, as icy surfaces of satellites of outer planets, trans-Neptunian objects, and comets, and in dense molecular clouds, where gas-phase species condensate onto dust grains.

Finally, in the interstellar medium the main electron production channel is given by cosmic-ray ionization of molecular hydrogen. The electrons emitted in this process have an initial average energy of about 30 eV. When such electrons generated in the gas phase interact with micron-thick ices, they would be essentially limited to the ice boundary surface. In X-ray-dominated regions, photons penetrate deeply within icy dust mantles, activating a bulk chemistry competing with surface processes.

This work was supported by the NSC grant NSC99-2112-M-008-011-MY3 (Yih) and the NSF Planetary Astronomy Program under Grant AST-1108898 (Chen). We are grateful to the former Director of OAPA, Dr. S. Sciortino, for the financial support to our research activity.

This work was also financially supported by Spanish MICINN/MINECO under projects AYA2008-06374 and AYA2011-29375 and CONSOLIDER grant CSD2009-00038; A.J.E. was supported by a research training grant from INTA; and the Autonomous Region of Sardinia, Project CRP 26666 (Regional Law 7/2007, Call 2010).

REFERENCES

Andrade, D. P. P., Rocco, M. L. M., & Boechat-Roberty, H. M. 2010, MNRAS, 409, 1289
Baratta, G. A., Castorina, A. C., Leto, G., et al. 1994, P&SS, 42, 759
Barnett, I. L., Lignell, A., & Gudipati, M. S. 2012, ApJ, 747, 13
Bennett, C. J., Chen, S.-H., Sun, B.-J., Chang, A. H. H., & Kaiser, R. I. 2007, ApJ, 660, 1588
Bennett, C. J., & Kaiser, R. I. 2007, 661, 899
Bouchiha, D., Gorfinkiel, J. D., Caron, L. G., & Sanche, L. 2007, JPhB, 40, 1259
Chen, Y.-J., Nuevo, M., Hsieh, J.-M., et al. 2007, A&A, 464, 253
Ciaravella, A., Muñoz Caro, G. M., Jiménez Escobar, A., et al. 2010, ApJ, 722, L45
Cruz Diaz, G. A., Muñoz Caro, G. M., Chen, Y.-J., & Yin, T.-S. 2013, A&A, submitted
de Barros, A. L. F., Domaracka, A., Andrade, D. P. P., et al. 2011, MNRAS, 418, 1363
D'Hendecourt, L. B., & Allamandola, L. J. 1986, A&AS, 64, 453
Feigelson, E. D., Gaffney, J. A., Garmire, G., Hillenbrand, L. A., & Townsley, L. 2003, ApJ, 584, 911
Gerakines, P. A., Schutte, W. A., & Ehrenfreund, P. 1996, A&A, 312, 289
Harris, T. D., Lee, D. H., Blumberg, M. Q., & Arumainayagam, C. R. 1995, JPhCh, 99, 9530
Hempelmann, A., Piancastelli, M. N., Heiser, F., et al. 1999, JPhB, 32, 2677
Henke, B. L., Gullikson, E. M., & Davis, J. C. 1993, ADNDT, 54, 181
Jiang, G. J., Person, W. B., & Brown, K. G. 1975, JChPh, 64, 1201
Leurini, S., Schilke, P., Wyronski, E., & Menten, K. M. 2007, A&A, 466, 215
Milligan, D. D., & Jacox, M. E. 1971, JChPh, 54, 927
Mumma, M. J., & Charnley, S. B. 2011, ARA&A, 49, 471
Öberg, K. I., Garrod, R. T., van Dishoeck, E. F., & Linnartz, H. 2009a, A&A, 508, 891
Öberg, K. I., Boogert, A. C., Pontoppidan, K. M., et al. 2011, ApJ, 740, 109
Öberg, K. I., van Dishoeck, E. F., & Linnartz, H. 2009b, A&A, 496, 281
Pilling, S., Neves, R., Santos, A. C. F., & Boechat-Roberty, H. M. 2007, A&A, 464, 393

Rejoub, R., Morton, C. D., Lindsay, B. G., & Stebbings, R. F. 2003, JChPh, 118, 1756
Ribas, I., Guinan, E. F., Gudel, M., & Audard, M. 2005, ApJ, 622, 680
Schutte, W. A., Allamandola, L. J., & Sandford, S. A. 1993, Icar, 104, 118
Sullivan, K. K. 2012, Honors Thesis Collection, Wellesley College
Vinodkumar, M., Korot, K., & Vinodkumarc, P. C. 2011, IJMSp, 305, 26
Vinodkumar, M., Limbachiya, C., Joshipura, K. N., Vaishnav, B., & Gangopadhyay, S. 2008, JPhCS, 115, 012013
Wexler, A. S. 1967, ApSRv, 1, 29
Whittet, D. C. B., Cook, A. M., Herbst, E., Chiar, J. E., & Shenoy, S. S. 2011, ApJ, 742, 28
Yamada, H., & Person, W. B. 1964, JChPh, 41, 2478